Scaled behavior of interface waves at an imperfect solid-solid interface

Tony Valier-Brasier, Thomas Dehoux, and Bertrand Audoin[a)]
University of Bordeaux, I2M, UMR 5295, F-33400 Talence, France, and CNRS, I2M, UMR 5295, F-33400 Talence, France

(Received 21 March 2012; accepted 1 June 2012; published online 19 July 2012)

Laser ultrasonic techniques allow the remote analysis of adhesion mechanisms at imperfect interfaces up to GHz frequencies. However, the sensitivity of interface waves to the properties of the contact is not very well known. In the present work, the mechanical boundary conditions are described considering that the contacting solid half-spaces are connected by tangential and normal springs. Such a modeling implies a discontinuity of the displacement field across the interface. To identify the relative amplitudes of the different types of interface waves—skimming, leaky Rayleigh (LR) and Stoneley (St) waves—a semi-analytical time domain model describing the thermoelastic laser generation is derived. The results illustrate the influence of the boundary conditions on the attenuation of the LR wave and on the existence of the St wave. In addition, a single compact and elegant dispersion equation is presented to investigate the behaviour of the interface waves propagating along a generalized imperfect boundary. Such analysis reveals the existence of a cutoff frequency f_c close to which the St wave behaves like a skimming transverse wave. A scaled analysis demonstrates that two master curves suffice to describe the dispersion of LR and St waves and that f_c is inversely proportional to the tangential interfacial spring constant.
 [http://dx.doi.org/10.1063/1.4733949]

I. INTRODUCTION

Assessing the quality of interfaces is of the utmost importance for the design and evaluation of bonded structures, microelectronic devices,[1] coatings, or even for the optimization of cell adhesion on biomaterials.[2] Yet the presence of cracks, roughness or porosities, residual stresses, or diffusion interlayer[3] often hinders the functioning of these materials. The development of characterization techniques is therefore a critical requirement in tribology, microelectronics, thin film science, and in bioengineering. To this end, a large number of destructive methods have been developed, such as scratch or peel tests, indentation, or laser spallation techniques.[4]

Acoustic-based methods are of great interest since they provide a non-destructive mean to probe interface quality and adhesion. Techniques using reflection and transmission of bulk acoustic waves at an imperfect interface[3,5–7] or propagation of guided waves in bonded structures[8–12] or in plates with delamination[13–16] have been developed. Although less used, the application of interface waves suggests interesting potentialities owing to their extreme sensitivity to the boundary conditions at the contacting interface.[17–19]

To infer the quality of the interface from the acoustic propagation, it is necessary to introduce dynamic boundary conditions. A classical approach considers that the two contacting materials are connected by a spring of constant K.[5] Such a modeling leads to a discontinuity of the displacements Δu across the interface, while the stresses remain continuous and equal to $K\Delta u$. This modeling has been used to describe the acoustic propagation across thin interlayers,[5,7,20] rough interfaces,[9,21,22] or cracks.[23,24] Complex-valued spring constants can also be used in order to model viscous effects.[25–27] A discontinuity of the normal displacements can be introduced, as well as of the tangential displacements to consider interface imperfections appearing upon shearing.[7,8,28] Moreover, anisotropic interfaces can be modelled with three spring constants, a normal spring constant and two tangential ones.[15]

Regarding interface waves propagating along the interface between two different isotropic half-spaces in contact, several works have reported on the analytical determination of the interface waves velocity for a welded interface[29] or a slip interface.[30] In such cases, interface waves of two different kinds may exist: the Stoneley (St) wave and the Leaky Rayleigh (LR) wave. The St wave exists only in a narrow range of material pairs in the case of welded interface and for a wider range in the case of a slip interface.[17,25] However, these boundary conditions are limiting cases, and the influence of the spring stiffnesses on the interface waves are not known. When the contacting materials are identical—typically along fracture lips—the existence of dispersive unattenuated symmetric and antisymmetric "fracture" interface waves has been demonstrated.[19,31] The existence of the fastest of these waves depends on the normal spring constant and that of the slowest wave on the tangential spring constant.

The purpose of the present work is to consider the general case of two different isotropic solid half-spaces in contact. The imperfect interface is here described by both normal and tangential spring constants, in order to investigate interface wave dispersion as well as the existence of the St wave.

At low frequencies, the spring constant $K = C/l$ modeling the interface can alternatively be seen as a thin layer of thickness l and of rigidity C. The length l can either describe

[a)]Electronic mail: b.audoin@u-bordeaux1.fr.

the thickness of a thin interfacial layer,[7,20] the width of a fracture,[24,31] or the average height of the asperities of a rough interface.[9,21,22] In geophysics, owing to the poor adhesion of terrestrial layers and to the large scale of interfacial asperities, low spring constants (between 10^8 and 10^{12} Pa m^{-1}) are considered at frequencies $\lesssim 1$ kHz.[24] In nondestructive testing of millimeter structures, higher spring constants (between 10^{15} and 10^{18} Pa m^{-1}) are studied at ≈ 400 MHz.[32] Considering the propagation of GHz bulk longitudinal waves across interfaces of nanometer characteristic lengths, spring constants up to 10^{19} Pa m^{-1} are found.[3,33] To test nano-interfaces of high stiffness with high sensitivity, it is therefore required to propagate interface waves of GHz frequencies.

Interface waves can be generated by conversion of bulk or surface acoustic wave[18,34–36] with limited efficiency and requiring an uncoated portion of the sample. If one of the contacting media is transparent, interface waves can also be generated thermoelastically by the absorption of a short laser pulse at the interface.[37,38] The present work concerns this latter configuration. Such a laser ultrasonics technique (LU) is non-contact and allows the remote generation of GHz frequencies.[39,40]

In a previous paper,[41] a semi-analytical model has been developed to describe the thermoelastic generation of elastic waves in an anisotropic half-space. This model is here extended in Sec. II to consider the case of two half-spaces separated by a generalized imperfect interface. To further investigate the predictions of this model, the corresponding dispersion equations of harmonic interface waves are calculated in Sec. III. Numerical results are analyzed in Sec. IV, and a scaled analysis of the dispersion of interface waves is proposed in Sec. V.

II. MODELING OF THERMOELASTIC PROCESSES AT A GENERALIZED IMPERFECT INTERFACE BETWEEN TWO ANISOTROPIC SOLIDS

Several models for the generation of elastic waves in an anisotropic half-space by transient point or line sources have been developed.[41–45] Although the case of the thermoelastic generation of interface waves at the perfect interface between a perfect fluid half-space and an isotropic solid half-space has been largely studied,[46–48] investigations of two isotropic solid half-spaces in contact remain scarce.[40] In this section, we propose an even more general modeling of the thermoelastic generation at the interface formed by two anisotropic viscoelastic half-spaces. In addition, imperfect interface quality is modeled by normal and tangential interfacial spring constants.[7,8,28]

The laser absorption causes a localized temperature rise, which in turn generates elastic waves by thermo-elastic coupling. In this section, the equations governing these phenomena are solved analytically in the wavenumber-frequency space, considering appropriate boundary conditions.

A. Governing equations

Two semi-infinite anisotropic viscoelastic media are separated by a plane interface located at $x_1 = 0$ in Cartesian

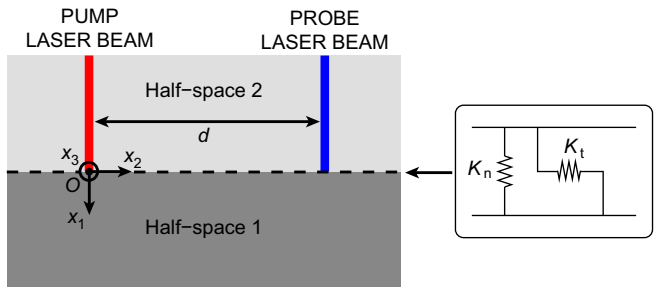

FIG. 1. Geometry (left) and symbolic representation of the interface (right).

coordinates (x_1, x_2, x_3) (see Fig. 1). Index $i = 1, 2$ stands for the medium located at $x_1 > 0$ and $x_1 < 0$, respectively. The origin O is chosen to coincide with the center of the pump laser spot. The absorption of the pump light in medium 1 leads to a sudden localized temperature rise. Assuming the temperature is not affected by acoustic propagation, the photothermally induced temperature rise $T^{(i)}$ in medium i is described by the heat diffusion equation

$$\rho^{(i)} C_p^{(i)} \frac{\partial T^{(i)}}{\partial t} = \nabla \cdot \left(\bar{\kappa}^{(i)} \nabla T^{(i)} \right) + Q^{(i)}, \tag{1}$$

where $\rho^{(i)}$, $C_p^{(i)}$, and $\bar{\kappa}^{(i)}$ are the mass density, heat capacity, and thermal conductivity tensor, respectively. The source term $Q^{(i)}$ describes the absorption of the pump laser beam.

The displacement field $\mathbf{u}^{(i)}$ is solution of the equation of motion

$$\rho^{(i)} \frac{\partial^2 \mathbf{u}^{(i)}}{\partial t^2} = \mathrm{div} \bar{\sigma}^{(i)}, \tag{2}$$

where the components $\sigma_{kl}^{(i)}$ of the stress tensors are[45]

$$\sigma_{kl}^{(i)} = C_{klmn}^{(i)} \frac{\partial u_m^{(i)}}{\partial x_n} - \lambda_{kl}^{(i)} T^{(i)}. \tag{3}$$

A Kelvin-Voigt model[49] is considered to derive the frequency dependence of the complex components $C_{klmn}^{(i)}$ of the viscoelasticity tensor. The tensor $\bar{\lambda}^{(i)}$ is defined as the product of $\bar{\bar{C}}^{(i)}$ and of the thermal dilatation tensor $\bar{\alpha}^{(i)}$. The thermal stress $\bar{\lambda}^{(i)} T^{(i)}$ thereby appearing in Eq. (3) is the thermoelastic source in the propagation equation, Eq. (2).

To allow laser generation at the interface, medium $i = 2$ is considered transparent, and the source term $Q^{(2)}$ in Eq. (1) is zero. To describe the generation by a point-source, transversely isotropic media with a symmetry plane parallel to the boundary $x_1 = 0$ is considered. We first model a photothermal source focused to a line along $\mathbf{x}_3$ with an optical absorption in medium $i = 1$ along $\mathbf{x}_1$. The source term $Q^{(1)}$ therefore takes the following form:

$$Q^{(1)}(x_1, x_2, t) = \beta^{(1)} I G_\chi(x_2) G_\tau(t) \mathrm{e}^{-\beta^{(1)} x_1}, \tag{4}$$

where I is the electromagnetic energy per unit length absorbed in medium 1, and $\beta^{(1)}$ is the inverse of the optical skin depth. Functions G_χ and G_τ describing the lateral and time distributions of the laser pulse intensity are Gauss functions

$$G_a(x) = \frac{1}{a}\sqrt{\frac{4ln(2)}{\pi}}e^{-4ln(2)x^2/a^2} \tag{5}$$

of full width at half maximum (FWHM) $a = \chi, \tau$, respectively.

Owing to symmetry, $\mathbf{u}^{(i)}$ and $T^{(i)}$ do not depend on x_3. Since the line source is focused along $\mathbf{x_3}$ in the symmetry plane, $u_3^{(i)} = 0$. The spectrum of the normal displacement $\hat{u}_1^{(i)}(x_1, k_2, \omega)$ corresponding to this line source is calculated from the semi-coupled Eqs. (1) and (2) in the frequency-wavelength domain using a double inverse Fourier transform, with k_2 and ω the dual variables of x_2 and t, respectively. The solution of Eqs. (1) and (2) for a point-source is obtained from $\hat{u}_1^{(i)}(x_1, k_2, \omega)$ using a double Fourier-Hankel transform[50]

$$u_1^{(i)}(x_1, x_2, t) = \frac{1}{(2\pi)^2}\int_{-\infty}^{+\infty}\int_0^{+\infty}\hat{u}_1^{(i)}(x_1, k_2, \omega)J_0(-k_2x_2) \times e^{j\omega t}k_2 dk_2 d\omega, \tag{6}$$

where J_0 is the zero-order Bessel function of the first kind.[51] The same method can be applied to the other components of the displacement, using higher-order Bessel functions.[52]

B. Displacement of the imperfect interface in the frequency-wavenumber domain

The heat diffusion equation, Eq. (1), in the dual space (ω, k_2) is a second order differential equation. The solution for each medium i therefore takes the form[41]

$$\hat{T}^{(i)}(x_1) = \sum_{q=\beta^{(i)},\Gamma^{(i)}} \hat{T}_q^{(i)}\exp[(-1)^i q x_1]. \tag{7}$$

$\Gamma^{(i)} = (j\omega\rho^{(i)}C_p^{(i)}/\kappa^{(i)} + k_2^2)^{1/2}$ is the thermal wavenumber, where the components of the thermal conductivity tensor are such that $\kappa_{kl}^{(i)} = \kappa^{(i)}\delta_{kl}$. A perfect thermal contact is modeled by considering that the temperature field and heat flux are continuous across the interface $x_1 = 0$,

$$\begin{cases} \hat{T}^{(1)} = \hat{T}^{(2)}, & \text{(8a)} \\ \kappa^{(1)}\dfrac{\partial\hat{T}^{(1)}}{\partial x_1} = \kappa^{(2)}\dfrac{\partial\hat{T}^{(2)}}{\partial x_1}. & \text{(8b)} \end{cases}$$

Detailed expressions of $\hat{T}_q^{(i)}$ appearing in Eq. (7) are given in Appendix A 1.

Under such an assumption, the temperature field is not affected by the quality of the interface. The influence of the interface on the temperature could be modeled by introducing a thermal resistance, the so-called Kapitza resistance.[53,54] However, the effects of a thermal resistance on the GHz elastic waves are considered negligible.[33]

Similarly, the solutions of the equation of motion, Eq. (2), in the dual space (ω, k_2) are sum of homogeneous solutions $\hat{\mathbf{U}}_h^{(i)}$ and of particular solutions $\hat{\mathbf{U}}_p^{(i)}$. Given the source term $\nabla\cdot(\bar{\lambda}^{(i)}T^{(i)})$ in Eq. (2), the particular solutions take the form of the temperature field,

$$\hat{\mathbf{U}}_p^{(i)} = \sum_{q=\beta^{(i)},\Gamma^{(i)}} \hat{\mathbf{U}}_q^{(i)}\exp[(-1)^i q x_1], \tag{9}$$

where each $\hat{\mathbf{U}}_q^{(i)}$ $(q = \beta^{(i)}, \Gamma^{(i)})$ is obtained from Eq. (2) in the dual space (ω, k_2), independently of the mechanical boundary conditions (see Appendix A 2).

Owing to Snell's law, wave vector component k_2 in the direction $\mathbf{x}_2$ is the same for all waves in both media. The wave vector components $k_{n_1}^{(i)}$ in the direction $\mathbf{x}_1$ for longitudinal $(n = L)$ and transverse $(n = T)$ plane waves are obtained by solving the Christoffel equation. Consequently, each component of the spectrum of the homogeneous solution $\hat{\mathbf{U}}_h^{(i)}$ is expressed as a sum of longitudinal and transverse plane waves of wave vector components $k_{n_1}^{(i)}$[41]

$$\hat{\mathbf{U}}_h^{(i)}(x_1) = \sum_{n=L,T}\hat{\mathbf{U}}_n^{(i)}\hat{\zeta}_n^{(i)}e^{(-1)^i jk_{n_1}^{(i)}x_1}, \tag{10}$$

Detailed expressions for $k_{n_1}^{(i)}$ and for the polarization vectors $\hat{\mathbf{U}}_n^{(i)}$ are given in Appendix A 2. Bulk wave amplitudes $\hat{\zeta}_n^{(i)}$ are then calculated in each solid from mechanical boundary conditions describing imperfect interfaces.

The quality of the interface is described by a spring model,[8,23,28] leading to a discontinuity of the displacement fields and continuity of the stresses across the interface. This model is represented schematically in Fig. 1. Expressions of the normal $\sigma_{11}^{(i)}$ and tangential $\sigma_{12}^{(i)}$ stresses are obtained by replacing the expressions of the temperature and displacements fields given by Eqs. (7), (9), and (10) into Eq. (3) (see Appendix A 3). The stresses in each media $i = 1, 2$ are related by the following boundary conditions:

$$\begin{cases} \hat{\sigma}_{11}^{(1)} = \hat{\sigma}_{11}^{(2)} = K_n\left(\hat{U}_1^{(1)} - \hat{U}_1^{(2)}\right), & \text{(11a)} \\ \hat{\sigma}_{12}^{(1)} = \hat{\sigma}_{12}^{(1)} = K_t\left(\hat{U}_2^{(1)} - \hat{U}_2^{(2)}\right), & \text{(11b)} \end{cases}$$

where K_n and K_t are the normal and tangential spring constants, respectively. $\hat{U}_s^{(i)}$ are the components of the displacement field in medium i along direction s calculated at the boundary $x_1 = 0$. Note that the general case of anisotropic interfaces must be modelled with three spring constants, a normal spring constant and two tangential ones.[15] However, owing to the symmetry of the wave generation for a line source and two transverse isotropic solids, no displacement u_3 is involved and only one spring constant K_t is necessary.

The spring model has three limiting cases. If $K_n = K_t = 0$, the interface $x_1 = 0$ is an unbounded interface corresponding to two free surfaces without mechanical contact. In the case where $K_n \to \infty$ and $K_t = 0$, the normal stresses being finite quantities, the normal displacements $\hat{U}_1^{(i)}$ are continuous and the shear stresses are zero at the interface. The spring model therefore approaches a slip interface. In the case where $K_n \to \infty$ and $K_t \to \infty$, the normal and tangential stresses being finite quantities, the normal and tangential displacements are continuous at the interface. The spring model therefore approaches a welded interface.

Once the amplitudes of the displacement components are obtained using the boundary conditions, Eq. (11), a numerical inverse Fourier transform is performed to evaluate the spatio-temporal evolution of the normal displacement. Since the

reflective medium $i = 1$ is that of experimental access, the normal displacement $u_1^{(1)}(x_1 = 0)$ in medium $i = 1$ is calculated. Such calculations include notably LR and St waves. Yet, to identify these waves from $u_1^{(1)}$, it is necessary to calculate the velocity of each interface wave. To this end, dispersion equations accounting for the imperfect interface between isotropic solids are introduced and solved in Sec. III.

III. DISPERSION EQUATIONS FOR INTERFACE WAVES PROPAGATING ALONG AN IMPERFECT INTERFACE

To supplement the results of the time modeling presented in Sec. II, dispersion curves of interface waves must be plotted for different types of interface. Due to the complexity of the calculations of interface waves dispersion equations for anisotropic solids in the case of welded[55–58] and slip[59,60] interfaces, this section is restricted to the dispersion curves for isotropic materials. For this reason, a formalism based on Lamé parameters is used hereafter.

Several authors have studied the dispersion curves of the welded interface,[18,35,61] the slip interface,[30,40] and the spring model[34] separately. Such analyses have led to a dispersion equation for each case. However, the relations between all these dispersion curves has never been derived. In this section, we introduce a new type of interface, the so-called grip interface. We thereby propose a single compact and elegant dispersion equation for interface waves at a free, welded, slip, or grip interface.

The solving of the boundary conditions for harmonic waves leads to a linear system of equations. The dispersion equations correspond to the vanishing of the determinant of such a system, the so-called characteristic determinant. The boundary conditions depend on the quality of the interface and involve the normal and tangential displacements, and the normal and tangential stresses. The aim of this section is to derive the relations between the determinants associated to each interface quality. For this purpose, the determinants of each limiting case of the spring model are first introduced.

The time-harmonic displacement fields of angular frequency ω in each solid $i = 1, 2$ are solutions of the equation of motion,

$$\rho^{(i)}\omega^2\tilde{\mathbf{u}}^{(i)} + \mathrm{div}\tilde{\bar{\sigma}}^{(i)} = \mathbf{0}, \tag{12}$$

where the components of the stress tensor are given by Hooke's law,

$$\tilde{\sigma}_{kl}^{(i)} = \lambda^{(i)}\mathrm{div}\tilde{\mathbf{u}}^{(i)}\delta_{kl} + \mu^{(i)}\left(\frac{\partial\tilde{u}_k^{(i)}}{\partial x_l} + \frac{\partial\tilde{u}_l^{(i)}}{\partial x_k}\right) \tag{13}$$

and where $\lambda^{(i)}$ and $\mu^{(i)}$ are Lamé constants. The grapheme tilde here denotes harmonic quantities.

The interface waves propagating at the interface between two isotropic solid half-spaces are linear combinations of longitudinal and shear waves of both solids. Interface waves have a wavenumber k in the direction of propagation $\mathbf{x}_2$ and a phase velocity $V = \omega/k$. The index 2 is omitted for k in this section to denote the wave number of interface waves exclusively. The time-harmonic displacement fields in media $i = 1, 2$ are[62]

$$\tilde{\mathbf{u}}^{(i)} = \begin{pmatrix} \tilde{U}_1^{(i)}(x_1) \\ \tilde{U}_2^{(i)}(x_1) \end{pmatrix} \mathrm{e}^{j(\omega t - kx_2)}, \tag{14}$$

with

$$\begin{pmatrix} \tilde{U}_1^{(i)}(x_1) \\ \tilde{U}_2^{(i)}(x_1) \end{pmatrix} = \begin{pmatrix} 1 \\ (-1)^{i+1} j\dfrac{1}{b_L^{(i)}} \end{pmatrix} \tilde{U}_L^{(i)} \mathrm{e}^{(-1)^i k b_L^{(i)} x_1} + \begin{pmatrix} 1 \\ (-1)^{i+1} j b_T^{(i)} \end{pmatrix} \tilde{U}_T^{(i)} \mathrm{e}^{(-1)^i k b_T^{(i)} x_1}, \tag{15}$$

where $\tilde{U}_L^{(i)}$ and $\tilde{U}_T^{(i)}$ are the amplitudes of the longitudinal and transverse bulk waves in both solids, respectively, and

$$b_n^{(i)} = \sqrt{1 - \left(\frac{V}{V_n^{(i)}}\right)^2}, \tag{16}$$

$V_L^{(i)} = \sqrt{(\lambda^{(i)} + 2\mu^{(i)})/\rho^{(i)}}$ and $V_T^{(i)} = \sqrt{\mu^{(i)}/\rho^{(i)}}$ being the bulk longitudinal and shear wave velocities, respectively.

Replacing Eqs. (14) and (15) in Hooke's law, Eq. (13), leads to the expressions of the normal $\tilde{\sigma}_{11}^{(i)}$ and tangential $\tilde{\sigma}_{12}^{(i)}$ stresses in both media at $x_1 = 0$,

$$\begin{cases} \tilde{\sigma}_{11}^{(i)} = (-1)^i \mu^{(i)} k \left[(2 - \zeta_i{}^2)\dfrac{\tilde{U}_L^{(i)}}{b_L^{(i)}} + 2b_T^{(i)}\tilde{U}_T^{(i)}\right], & \text{(17a)} \\ \tilde{\sigma}_{12}^{(i)} = -jk\mu^{(i)}[2\tilde{U}_L^{(i)} + (2 - \zeta_i{}^2)\tilde{U}_T^{(i)}]. & \text{(17b)} \end{cases}$$

where $\zeta_i = V/V_T^{(i)}$.

When the materials are perfectly unbounded, there is no interface anymore but two uncoupled free surfaces instead, which can independently support a Rayleigh wave. The characteristic determinant for each free surface, defined by $\sigma_{11}^{(i)} = 0$ and $\sigma_{12}^{(i)} = 0$, is[62]

$$D_{\mathrm{R}}^{(i)} = (2 - \zeta_i^2)^2 - 4b_L^{(i)}b_T^{(i)}. \tag{18}$$

The characteristic determinant for the slip interface, defined by $\tilde{\sigma}_{11}^{(1)} = \tilde{\sigma}_{11}^{(2)}$, $\tilde{U}_1^{(1)} = \tilde{U}_1^{(2)}$ and $\tilde{\sigma}_{12}^{(1)} = \tilde{\sigma}_{12}^{(2)} = 0$, is[30]

$$D_{\mathrm{Slip}} = b_L^{(2)}\zeta_2^2 D_{\mathrm{R}}^{(1)} + m b_L^{(1)}\zeta_1^2 D_{\mathrm{R}}^{(2)}, \tag{19}$$

where $m = \mu^{(2)}/\mu^{(1)}$.

The characteristic determinant for the welded interface, defined by $\tilde{\sigma}_{11}^{(1)} = \tilde{\sigma}_{11}^{(2)}$, $\tilde{\sigma}_{12}^{(1)} = \tilde{\sigma}_{12}^{(2)}$, $\tilde{U}_1^{(1)} = \tilde{U}_1^{(2)}$ and $\tilde{U}_2^{(1)} = \tilde{U}_2^{(2)}$, is[61,63]

$$\begin{aligned} D_{\mathrm{Welded}} = {} & m^2(b_L^{(1)}b_T^{(1)} - 1)D_{\mathrm{R}}^{(2)} + (b_L^{(2)}b_T^{(2)} - 1)D_{\mathrm{R}}^{(1)} \\ & + 8mb_T^{(1)}b_L^{(1)}b_T^{(2)}b_L^{(2)} + 2m(2 - \zeta_1^2)(2 - \zeta_2^2) \\ & - 4m[(2 - \zeta_1^2)b_L^{(2)}b_T^{(2)} + (2 - \zeta_2^2)b_L^{(1)}b_T^{(1)}] \\ & + m\zeta_1^2\zeta_2^2[b_L^{(1)}b_T^{(2)} + b_T^{(1)}b_L^{(2)}]. \end{aligned} \tag{20}$$

In order to show the relation between the characteristic determinants, it is necessary to introduce a new boundary condition corresponding to the continuity of tangential stresses

and tangential displacements, and to the vanishing of normal stresses: $\tilde{\sigma}_{12}^{(1)} = \tilde{\sigma}_{12}^{(2)}$, $\tilde{U}_2^{(1)} = \tilde{U}_2^{(2)}$, and $\tilde{\sigma}_{11}^{(1)} = \tilde{\sigma}_{11}^{(2)} = 0$. The characteristic determinant of this interface is

$$D_{\text{Grip}} = b_T^{(2)} \zeta_2^2 D_{\text{R}}^{(1)} + m b_T^{(1)} \zeta_1^2 D_{\text{R}}^{(2)}. \tag{21}$$

The characteristic determinant for the general spring model, corresponding to the boundary conditions $\tilde{\sigma}_{11}^{(1)} = \tilde{\sigma}_{11}^{(2)} = K_n(\tilde{U}_1^{(1)} - \tilde{U}_2^{(1)})$ and $\tilde{\sigma}_{12}^{(1)} = \tilde{\sigma}_{12}^{(2)} = K_t(\tilde{U}_1^{(2)} - \tilde{U}_2^{(2)})$, is

$$D_{\text{Spring}} = m^2 D_{\text{R}}^{(1)} D_{\text{R}}^{(2)} - m\zeta_1 \left(\frac{\Omega_n}{\omega} D_{\text{Slip}} + \frac{\Omega_t}{\omega} D_{\text{Grip}} \right) + \frac{\Omega_n \Omega_t}{\omega^2} \zeta_1^2 D_{\text{Welded}}, \tag{22}$$

where Ω_n and Ω_t are characteristic frequencies given by

$$\Omega_{n,t} = \frac{K_{n,t}}{\rho_{(1)} V_T^{(1)}}. \tag{23}$$

To deal with dimensionless equations, all determinants in Eq. (18) to (22) have been normalized by the second Lamé constant $\mu_{(1)}$ in medium 1. Consequently, $V_T^{(1)}$ appears in the expression of the characteristic frequencies instead of $V_T^{(2)}$. The meaning of $\Omega_{n,t}$ will be analyzed thoroughly in Sec. V.

Equations (18)–(21) are frequency-independent.[62] However, the general expression, Eq. (22), clearly shows that the interface waves are dispersive when taking the spring model into account.[19,31,34]

Two types of interface waves corresponding to the two roots of the dispersion equations can exist between two isotropic solid half-spaces: the St wave and the LR wave. The phase velocity V_{LR} of the LR wave is complex. On the contrary, the phase velocity V_{St} of the St wave is real. V_{St} and V_{LR} are not dispersive for the limiting cases (slip[30] and welded[61,63] interfaces) but become dispersive in the case of the spring model,[34] as shown in Eq. (22). Moreover, the St wave only exists in a narrow range of material pairs in the case of a welded interface[63] and in a wider range in the case of a slip interface.[17,25]

In Sec. IV, by analyzing simultaneously the results of the time domain model (Eq. (6) of Sec. II A) and of the dispersion equations, the dispersion of the Rayleigh wave will be discussed as a possible tool to characterize the quality of interfaces, and the existence of the St wave will be investigated in all interface cases.

IV. INFLUENCE OF THE BOUNDARY CONDITIONS ON THE INTERFACE WAVES

In order to analyze separately the influence of each interface spring (Fig. 1), two cases are studied. In the first case, the tangential and normal spring constants are such that $K_t = 0$ and $0 < K_n < \infty$, the quality of the interface being comprised between a free surface and a slip interface. In the second case, $K_n \to \infty$ and $0 < K_t < \infty$, the interface being comprised between a slip interface and a welded interface.

In both cases, the configuration evaluated numerically for illustration is a glass half-space on an aluminium half-space. We consider isotropic materials as a particular case of the anisotropic calculations presented in Sec. II. The wavelength of the pump laser beam is $\lambda_Q = 400$ nm. At this wavelength, the glass medium is transparent and the optical pump beam is only absorbed in aluminium over a skin depth $\beta^{-1} = 7$ nm. The pump laser beam is circular with a diameter (FWHM, Eq. (5)) $\chi = 1\ \mu$m. The pulse duration is $\tau = 100$ fs. The relevant mechanical and thermal properties are presented in Table I. The normal displacement $u_1^{(1)}$ in medium $i = 1$ is calculated at a position slightly below the interface $x = 0$ to avoid the numerical discontinuity imposed by the boundary conditions.

TABLE I. Mechanical and thermal properties.

Materials	Aluminium ($i = 1$)	Glass ($i = 2$)
$\rho^{(i)}$ (kg/m^3)	2700	2500
$C_{11}^{(i)}$ (GPa)	120	70
$C_{44}^{(i)}$ (GPa)	30	25
$C_p^{(i)}$ (J kg^{-1} m^{-3})	902	700
$\kappa^{(i)}$ (W m^{-1} K^{-1})	237	1.2
$\alpha^{(i)}$ (K^{-1})	25×10^{-6}	7×10^{-6}

A. K_t=0: from the free surface to the slip interface

In this section, the spring constant $K_t = 0$ and the spring K_n varies in the interval $[2, 2.10^4]$ GPa.μm^{-1}. The different interfaces corresponding to the discrete values of K_n are called I_k^n, as presented in Table II. Since the displacement of the reflective medium $i = 1$ surface is that of experimental access, the normal displacement $u_1^{(1)}$ is calculated at the interface $x_1 = 0$ for the different interfaces I_k^n and for the limiting cases, the free surface and the slip interface. In order to observe possible dispersion of the interface waves, $u_1^{(1)}$ is calculated for two pump-probe distances, $d = 10\ \mu$m and $d = 40\ \mu$m. For each type of interface, $u_1^{(1)}$ is normalized by the amplitude of the first interface wave (R, LR, or St, depending on interface quality) for the distance $d = 10\ \mu$m. These normal displacements are plotted vs time in Fig. 2. As d increases, the amplitudes of the acoustic pulses decrease owing to the circular shape of the laser source.

Only one wave is observed in Fig. 2 in the case of the free surface (top curve). This wave corresponds to the Rayleigh wave propagating in aluminium without attenuation and with a velocity $V_{\text{R}}^{(1)} = 3110$ m/s, matching that calculated from $D_{\text{R}}^{(1)}$ with Eq. (17). In the case of the slip interface (bottom curve), two waves are clearly visible: a longitudinal skimming wave and an interface wave. In the case of the slip interface for this pair of materials, Eq. (19) has two roots, $V_{St} = 3000$ m/s corresponding to the St wave and $V_{LR} = 3950 + j165$ m/s corresponding to the LR wave. Since both interface waves are non-dispersive, the observed acoustic pulse is

TABLE II. Normal spring constant K_n and corresponding interface I_k^n.

Interfaces	I_1^n	I_2^n	I_3^n	I_4^n	I_5^n	I_6^n	I_7^n	I_8^n	I_9^n	I_{10}^n
K_n (GPa/μm)	2	10	25	50	100	300	500	1000	5000	20 000

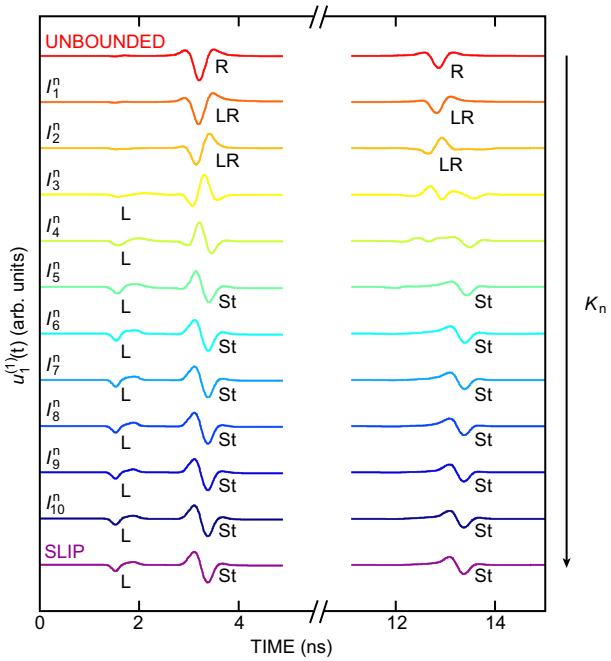

FIG. 2. Normalized normal displacements of the interface for pump-probe distances $d = 10\,\mu$m (left) and $d = 40\,\mu$m (right) for each interface I_k^n when $K_t = 0$.

associated to a St wave. For interfaces I_5^n to I_{10}^n, the shapes and arrival times of the acoustic pulses are approximately the same as in the case of the slip interface, meaning that the interface wave is a St wave. For interfaces I_1^n and I_2^n, the shape of the acoustic pulses is similar to that observed in the case of the free surface, meaning that the interface wave is a LR wave with low attenuation. However, for interfaces I_3^n and I_4^n, it is not possible to determine the type of interface waves because of the complicated shape of the acoustic pulse observed for $d = 40\ \mu$m. This shape results either from dispersion or from the superimposition of a St wave and of a LR wave with similar amplitudes.

To identify the corresponding waves, the phase velocity of the St wave and the real part of the phase velocity of the LR wave, obtained from dispersion equation, Eq. (22), are plotted vs frequency for each type of interface in Figs. 3 and

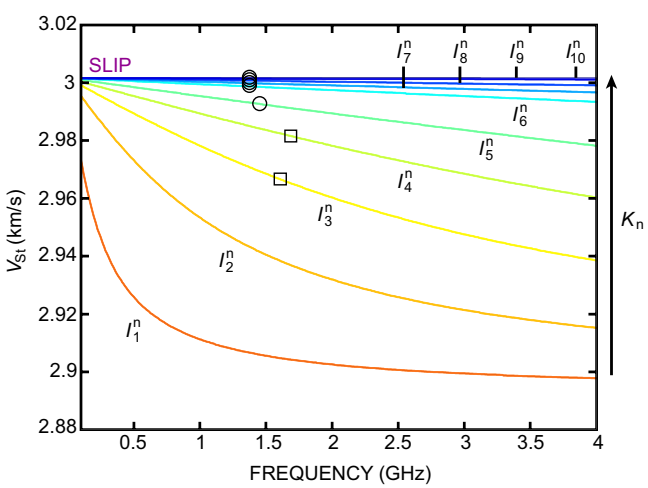

FIG. 3. Phase velocity of the St wave as a function of the frequency for each type of interface.

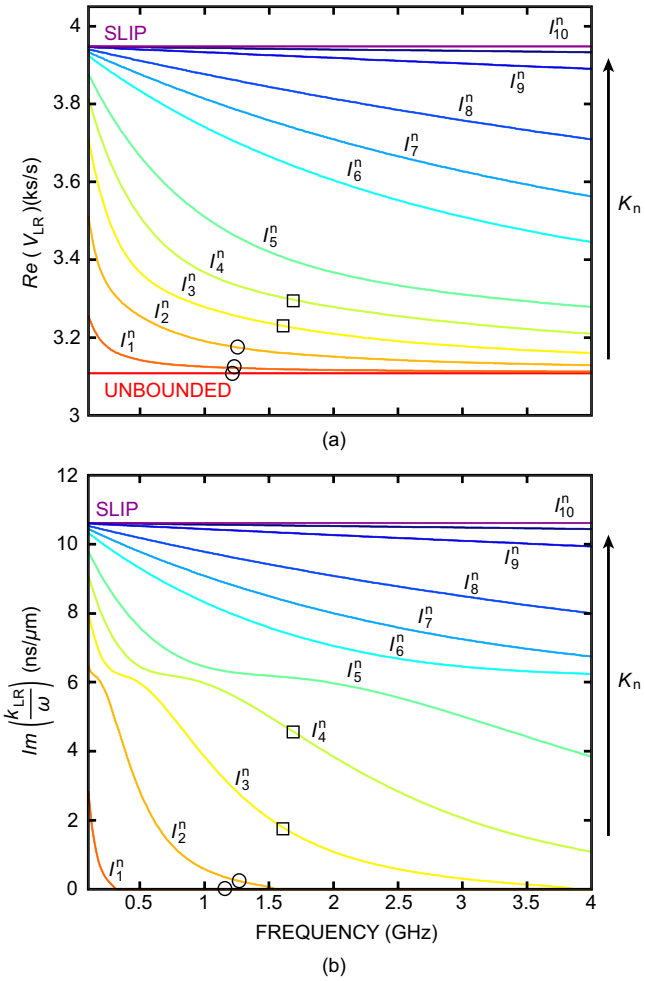

FIG. 4. (a) Real part of the phase velocity and (b) imaginary part of the complex wavenumber k_{LR} of the LR wave as functions of the frequency for the different types of interface.

4(a), respectively. Since the central frequencies of the interface waves observed in Fig. 2 are comprised between 1 and 1.5 GHz, the phase velocities are plotted for frequencies from 0.1 to 4 GHz. The central frequencies of the interface waves identified previously are indicated by circles and those of non-identified interface waves (interfaces I_3^n and I_4^n) by squares in Figs. 3 and 4(a).

As expected, the St waves for interfaces I_5^n to I_{10}^n, and the LR waves for interfaces I_1^n and I_2^n, are very little dispersive, supporting the fact that the shape of each wave pulse in Fig. 2 remains the same as that for the slip interface for interfaces I_5^n to I_{10}^n, and the same as for the free surface for interfaces I_1^n and I_2^n. More importantly, the St and the LR waves are also only slightly dispersive in the case of interfaces I_3^n and I_4^n, meaning that the acoustic pulses observed in Fig. 2 result actually from the superimposition of both St and LR waves. According to the quality of the interface, there is therefore a change of the type of laser-generated interface wave that can co-exist in the intermediary cases.

The St wave velocity variation $\Delta V_{St} = 110$ m/s observed in Fig. 3 is less than that of the real part of the LR wave velocity $\Delta\Re e[V_{LR}] = 840$ m/s observed in Fig. 4(a). To analyze the frequency-dependence of the attenuation of the LR wave, the ratio of the imaginary part of the wavenumber k_{LR} of the

LR wave to the angular frequency ω, $\Im m(k_{LR}/\omega)$, is plotted versus frequency in Fig. 4(b) for each type of interface. As expected, $\Im m(k_{LR}/\omega)$ is close to that for a free surface for the interfaces I_1^n and I_2^n, i.e., close to 0, and is close to that for a slip interface for the interfaces I_9^n and I_{10}^n. Moreover, $\Im m(k_{LR}/\omega)$ increases with the quality of the interface (with increasing K_n). The effects of the interface quality on the attenuation and velocity dispersion of the LR wave, as opposed to the slight dispersion of the St wave, demonstrate that they are relevant parameters to characterize adhesion between solids.

In this section, we have demonstrated that the type of interface wave generated depends greatly on the interface quality. Additionally, it has been shown that the velocity and attenuation of the LR wave are very sensitive to K_n in the case where $K_t = 0$. These observations can serve as tool for the assessment of interface quality for non-destructive purposes. The behaviour of the interface waves is now studied when the tangential spring constant K_t varies and the normal spring constant K_n is fixed.

B. $K_n \to \infty$: from the slip interface to the welded interface

In this section, the normal spring constant is fixed so that $K_n \to \infty$, and the tangential spring K_t is comprised in the interval $[2, 1000]$ GPa.μm^{-1}. The different interfaces corresponding to the discrete values of K_t are called I_k^t, as presented in Table III. The normal displacement of the interface calculated for different interfaces I_k^t and for the limiting cases, the slip interface and the welded interface are plotted in Fig. 5 for two pump-probe distances, $d = 10$ μm and $d = 40$ μm.

For each interface, two waves are clearly visible in Fig. 5, a skimming longitudinal wave and an interface wave. In the case of the slip interface, the interface wave is a St wave (see Sec. IV A). In the case of the welded interface for this pair of materials, Eq. (20) has only one root corresponding to the LR wave, and the St wave therefore does not exist. For interfaces I_3^t to I_5^t, the St and LR waves are superimposed, as explained in Sec. IV A. Thus, as observed previously in Fig. 2, the type of interface wave generated depends greatly on the quality of the interface.

To scrutinize the dispersive behavior of the interface waves, the phase velocity of the St wave and the real part of the phase velocity of the LR wave are plotted for each interface in Figs. 6 and 7(a), respectively. The imaginary part of the wavenumber k_{LR} of the LR wave is also plotted in Fig. 7(b) for each interface. The central frequencies of the identified interface waves are indicated by circles and those of non-identified interface waves by squares in Figs. 6 and 7(a).

TABLE III. Values of the tangential spring constant K_t and corresponding interface I_k^t.

Interfaces	I_1^t	I_2^t	I_3^t	I_4^t	I_5^t	I_6^t	I_7^t	I_8^t	I_9^t	I_{10}^t
K_t (GPa/μm)	2	5	10	20	50	100	200	400	750	1000

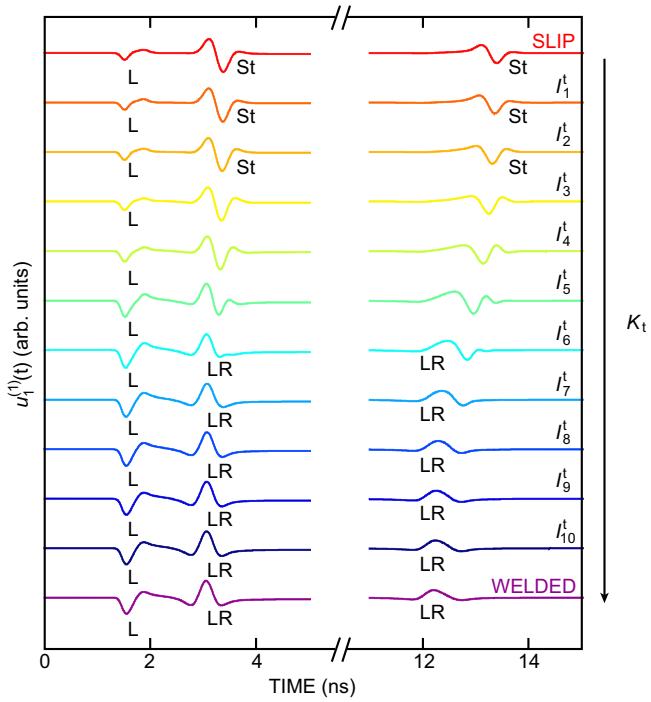

FIG. 5. Normalized normal displacements of the interface for the pump-probe distances $d = 10$ μm (left) and $d = 40$ μm (right) when $K_n \to \infty$.

When comparing the acoustic pulse shapes in Fig. 5 for interfaces I_1^t to I_3^t corresponding to pump-probes distances $d = 10$ μm and $d = 40$ μm, the behavior of the St waves tends to that in the case of the slip interface and is therefore only slightly dispersive. On the contrary, the acoustic pulse shape for interfaces I_7^t to I_{10}^t and for the welded interface show that the LR waves are very dispersive. Indeed the real part of the phase velocity of the LR wave decreases of a quantity $\Delta\Re e[V_{LR}] = 520$ m/s when the spring K_t increases. In addition, $\Im m(k_{LR}/\omega)$ varies largely between the slip interface and the welded interface. Thus, in this case again, the velocity dispersion and the attenuation of the LR wave are important parameters to characterize the contact at the interface.

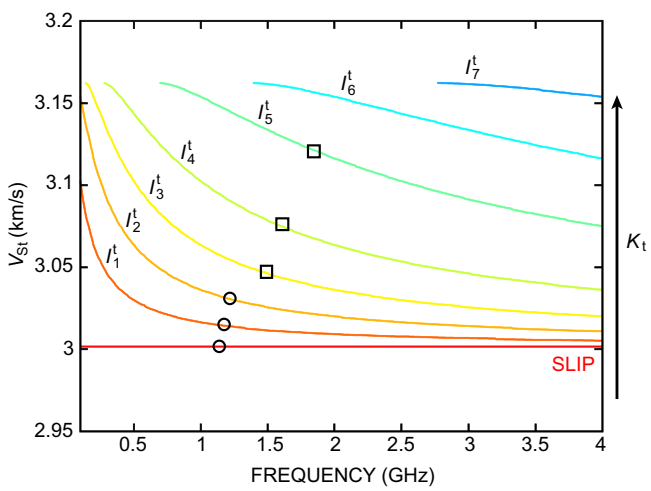

FIG. 6. Phase velocity of the St wave for each interface I_k^t.

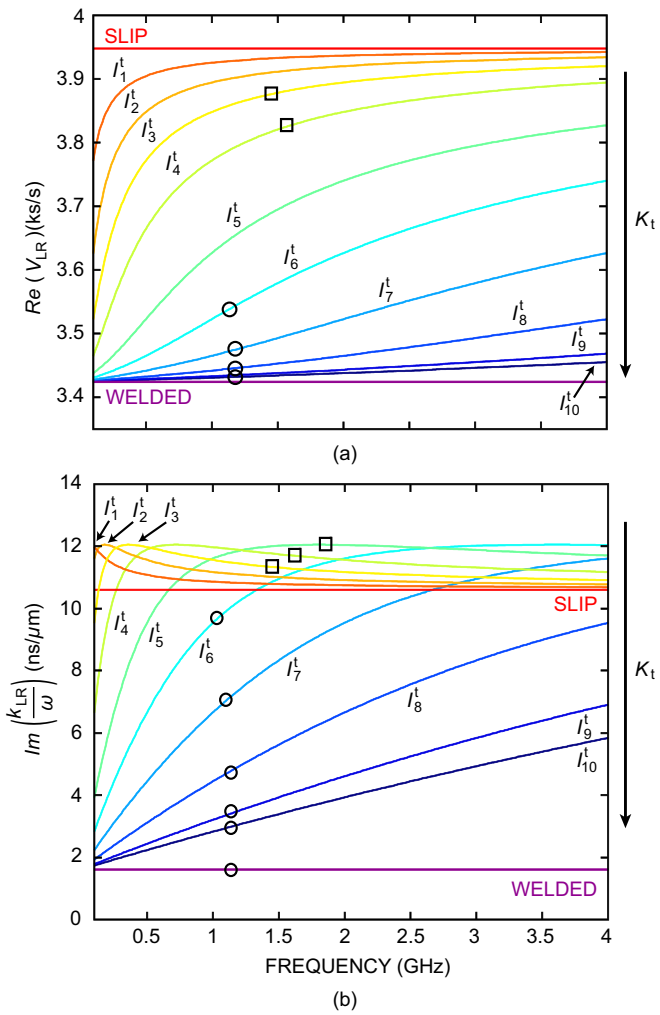

FIG. 7. (a) Real part of the phase velocity and (b) imaginary part of the complex wavenumber k_{LR} of the LR wave as functions of the frequency for each interface I_k^t.

However, this time a striking feature in the behaviour of the St waves is observed in Fig. 6. For the interfaces I_8^t to I_{10}^t, the St wave does not exist in the frequency range $[0.1, 4]$ GHz. Chadwick and Borejko have shown that the existence of the St wave depends on the Lamé constants and on the density of both materials. Our finding demonstrates that the existence of the St wave also greatly depends on the transverse spring constant. Moreover, for the interfaces I_3^t to I_7^t, a cut-off frequency f_c appears. The velocity of the St wave close to f_c approaches the lowest bulk shear wave velocity (in the present case, that of glass).[63,64]

As a conclusion, taking into account imperfect interfaces has demonstrated that, depending on the quality of the interface, there is a change of the type of interface wave generated. Moreover, the analysis of the dispersion curves has highlighted that the analysis of the LR wave velocity and attenuation can serve as a powerful tool to characterize the quality of an interface. Finally the most striking feature is the observation of cutoff frequencies close to which the St wave behaves like a skimming transverse wave, meaning that its existence depends on the transverse spring constant and on the driving frequency. Such behavior appeals for a scaled analysis of the dispersion curve.

V. SCALED BEHAVIOR OF INTERFACE WAVES

In the previous sections, the laser generation of interface waves at frequencies ~ 1 GHz has been analyzed using a time model. A comparison with the dispersion curves has shown an extreme sensitivity to spring constants close to $50\,\mathrm{GPa}.\mu\mathrm{m}^{-1}$ and has suggested the existence of a scaled behaviour.

Such a scaled behaviour has already been observed in the case of a fracture, acting like an interface between two identical materials, described with spring constants K_n and K_t. In such a case, two so-called fracture interface waves exist with different velocities.[19,31] The fast interface wave is independent of the spring constant K_t, whereas the slow interface wave is independent of the spring constant K_n. The characteristic frequencies for these interface waves are defined as[19]

$$\Omega_{n,t}^{frac} = \frac{K_{n,t}}{\rho V_{f,s}}, \tag{24}$$

where V_f and V_s are the phase velocities of the fast and slow interface waves, respectively. A similar expression has been derived for bulk waves.[28] However, the existence of characteristic frequencies in the case of interface waves propagating between different materials has never been demonstrated.

According to the type of interface studied, the relation between the spring constants are different. If the interface is equivalent to a thin film of viscous fluid (viscous slip bond), $K_t/K_n \ll 1$,[28] while for an interface between two compressed rough surfaces of same materials, $K_t/K_n = 0.71\,(1-\nu)/(2-\nu)$, where ν is Poisson's ratio.[65,66] Since characteristic frequencies depend on spring constants, it therefore appears important to scrutinize the evolution of interface waves dispersion curves when the ratio K_t/K_n varies.

In this section, we define characteristic frequencies in the case of interface waves propagating between different materials. We then analyze the dispersion of the interface waves around these frequencies in the general case where K_t/K_n varies.

A. Characteristic frequencies associated to the spring constants

In the case of an interface between different materials, the St and LR waves depend on both spring constants. By analogy with Eq. (24), the characteristic frequencies are here defined by Eq. (23). To analyse the meaning of these characteristic frequencies, the phase velocity of the St wave and the real part of the phase velocity of the LR wave in the case where $K_t = 0$ (corresponding to Figs. 3 and 4(a), respectively) are plotted versus the adimensional frequency f/Ω_n in Fig 8. All plots of the St wave velocity merge precisely into a single master curve and so do the LR waves.

As expected, for frequencies lower than Ω_n, the dispersion curves of the St and of the LR waves approach the phase velocity of the interface waves for the slip interface. When materials are the same, the phase velocities of the slow and fast fracture interface waves at high frequencies approach the Rayleigh wave velocity.[19] In the present case, the

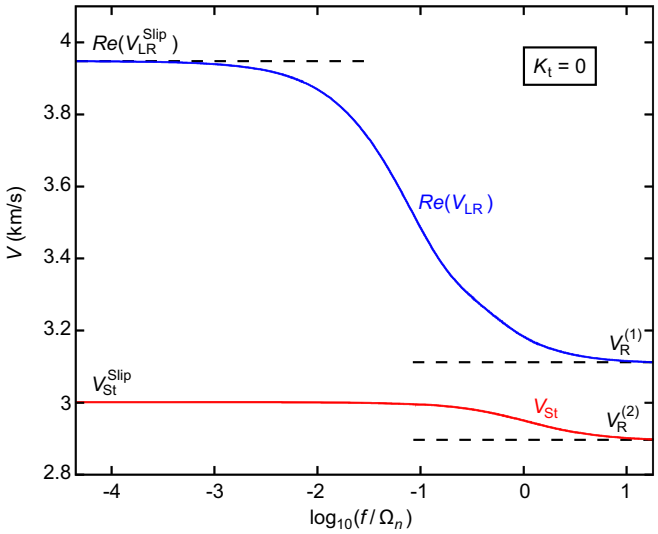

FIG. 8. Phase velocity of the St wave and real part of the phase velocity of the LR wave, Figs. 3 and 4(a), respectively, as functions of the adimensional frequency f/Ω_n.

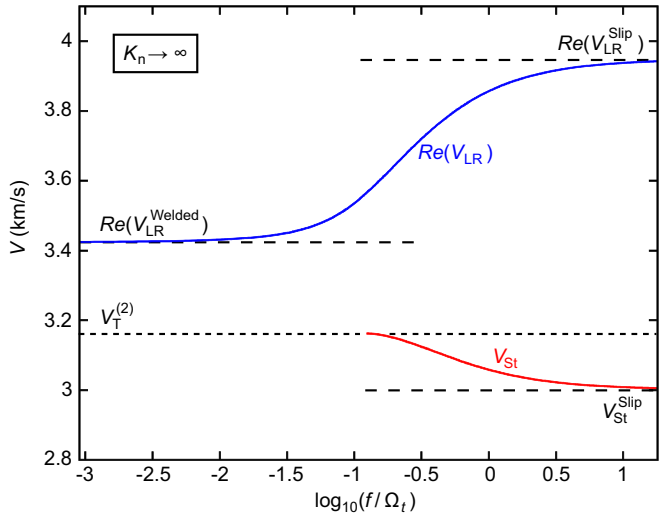

FIG. 9. Phase velocity of the St wave and real part of the phase velocity of the LR wave, Figs. 6 and 7(a), respectively, as functions of the adimensional frequency f/Ω_t.

behaviour of the phase velocity of interface waves is different. For frequencies larger than Ω_n, the dispersion curve of the LR wave approaches the largest Rayleigh wave phase velocity in either media and that of the St wave approaches the lowest Rayleigh wave phase velocity. Moreover, the St wave velocity varies in the interval $\log_{10}(f/\Omega_n) \in [-1, 1]$ and the real part of the LR wave velocity varies in the interval $\log_{10}(f/\Omega_n) \in [-2, 1]$, demonstrating that the frequency Ω_n indeed determines the transition between the slip and free interface behaviours.

This behaviour can be explained by analyzing the dispersion equation. The limit of the characteristic determinant of Eq. (22) when $K_t \to 0$ is

$$\lim_{K_t \to 0} D_{\text{Spring}} = m^2 D_R^{(1)} D_R^{(2)} - m\zeta_1 \frac{\Omega_n}{\omega} D_{\text{Slip}}. \tag{25}$$

For low frequencies D_{Spring} approaches the determinant D_{Slip}, and for high frequencies D_{Spring} approaches the product of the Rayleigh determinants $D_{\text{R}}^{(1)} D_{\text{R}}^{(2)}$. Between these limiting cases, the solution of the dispersion equation is a combination of the solutions for unbounded (i.e., Rayleigh waves) and slip interfaces.

In the case when $K_n \to \infty$, the phase velocity of the St wave and the real part of the phase velocity of the LR wave [see Figs. 6 and 7(a), respectively] are plotted versus the adimensional frequency f/Ω_t in Fig. 9. Here again, two master curves are obtained. As expected, for frequencies higher than Ω_t, both dispersion curves approach the phase velocity of the interface waves of the slip interface. For frequencies lower than Ω_t, the dispersion curve of the LR wave approaches the phase velocity of the LR waves for the welded interface and not the bulk shear wave velocity of one of the materials as mentioned in Refs. 19, 24, 31, and 67 for fracture interface waves. In this case, the frequency Ω_t determines the transition between the slip and welded interface behaviours.

This behaviour can be explained by analyzing the limit of the characteristic determinant of Eq. (22) when $K_n \to \infty$

$$\lim_{K_n \to \infty} \left(\frac{\omega}{\Omega_n} D_{\text{Spring}} \right) = -m\zeta_1 D_{\text{Slip}} + \zeta_1^2 \frac{\Omega_t}{\omega} D_{\text{Welded}}. \tag{26}$$

This expression shows that the determinant D_{Spring} approaches the determinant D_{Slip} at high frequencies and the determinant D_{Welded} at low frequencies.

Another interesting feature is that the St wave does not exist for frequencies lower than the cutoff frequencies f_c observed in Fig. 6. For frequencies close to f_c, the St wave velocity is close to the lowest bulk shear velocity, meaning that the latter is the high limiting value of the St wave velocity.[63] Moreover, as the ratio f_c/Ω_t remains constant, f_c is inversely proportional to the spring constant K_t.

B. Relation between spring constants

Let us now focus on the even more general case where both spring constants vary, as defined by the ratio $K_n/K_t = 10^\eta$ with $K_t = 1$ GPa.μm^{-1} and $\eta = 0...7$. The phase velocity of the St wave and the real part of the phase velocity of the LR wave are plotted vs f/Ω_t for the different values of η in Figs. 10(a) and 10(b), respectively. All dispersion curves show the same behaviour where three regimes are observed. The cutoff frequency of the St wave is the same as that observed previously and does not depend on K_n. The first regime corresponds to frequencies lower than the characteristic frequency Ω_t, for which the St wave velocity approaches the shear wave velocity in the slowest medium and the LR wave behaves as in the case of a welded interface. The second regime corresponds to frequencies between Ω_t and Ω_n for which the St and LR waves behave as in the case of the slip interface. For low values of η ($\eta = 0, 1, 2, 3$), the St and LR wave velocities do not reach the slip interface limit. The last regime corresponds to frequencies higher than Ω_n for which the St and LR wave velocities are equal to the lowest and to the largest Rayleigh wave phase velocity in either media, respectively.

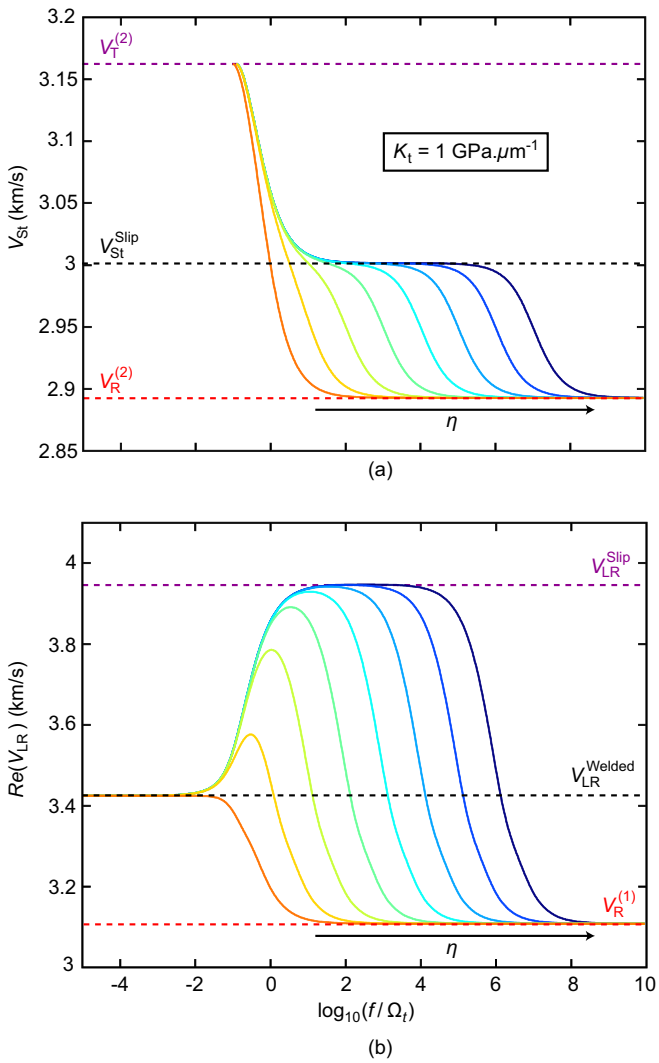

FIG. 10. (a) Phase velocity of the St wave and (b) real part of the phase velocity of the LR wave as functions of the adimensional frequency f/Ω_t.

VI. SUMMARY AND PERSPECTIVES

We have shown that the laser ultrasonics technique provides a non-destructive and non-contact mean to characterize interfaces. This technique allows high frequency interface waves to be generated, up to several GHz, well suited to the probing of interfaces of stiffnesses as high as 10^{19} Pa m^{-1}. It should prove useful when at least one of the materials is transparent, e.g., in microelectronics,[3] and in biology for the study of the adhesion of cells on biometallic implants.[68,69] Moreover, such a study is also relevant when wedge transducers are used to generate and detect interface waves remotely.

To describe the properties of the interface, the contacting solids have been assumed to be connected by tangential and normal springs. To identify the relative amplitudes of the St and LR waves, a time domain model based on the calculations of the temperature and elastic displacement fields has been developed. In addition, a single compact and elegant dispersion equation has been presented to investigate the behaviour of the interface waves propagating along a generalized imperfect boundary. The combination of these two approaches has allowed a scaled analysis, demonstrating that two master curves suffice to describe the dispersion of LR and St waves.

The simultaneous analysis of the numerical results of the time model and of the dispersion curves has demonstrated that the type of interface wave generated by the laser source is deeply related to the properties of the interface. Moreover, both normal and tangential interfacial stiffnesses induce phase velocity dispersion. This effect is remarkably noticeable on the real part of phase velocity—which is easily measurable—and on the attenuation of the LR wave. As the LR exists on wider range of material pairs than the St does, these observation define the LR wave as a extremely sensitive candidate to probe the quality of interfaces.

Furthermore, considering interfaces of intermediary qualities has revealed a nonmonotonic behavior of the phase velocities of the LR and St waves, owing to closely spaced normal and tangential characteristic frequencies. Such analysis has also revealed cutoff frequencies f_c below which the St wave does not exist. For frequencies close to f_c, the St wave velocity is close to the lowest bulk shear wave velocity in either media, meaning that the lowest bulk shear velocity is the high limiting value of the St wave velocity. The scaled analysis has also demonstrated that f_c is inversely proportional to the tangential interfacial stiffness and that it does not depend on the normal spring constant. These observations should allow a better understanding of the physical nature of the St waves and provide powerful tools for the assessment of the quality of interfaces. As a future work, the polarization of the St wave close to f_c will be analyzed.

ACKNOWLEDGMENTS

This work had been supported by the Agence Nationale pour la Recherche through grant PicoBio (ANR-07-BLAN-303).

APPENDIX A: PARTICULAR AND HOMOGENEOUS SOLUTIONS

1. Temperature fields

The medium $i = 2$ being transparent, the amplitude of the particular solutions in the dual space (ω, k_2) for the contacting solids are[41]

$$\begin{cases} \hat{T}_\beta^{(1)} = \dfrac{\beta^{(1)} I(1 - R_Q)}{\kappa^{(1)}[(\Gamma^{(1)})^2 - (\beta^{(1)})^2]}, & \text{(A1a)} \\ \hat{T}_\beta^{(2)} = 0. & \text{(A1b)} \end{cases}$$

Replacing the expressions of the temperature fields, Eq. (7), into the thermal boundary conditions, Eq. (8), leads to the amplitudes of the homogeneous solutions

$$\begin{cases} \hat{T}_\Gamma^{(1)} = -\dfrac{\kappa^{(1)}\beta^{(1)} + \kappa^{(2)}\Gamma^{(2)}}{\kappa^{(1)}\Gamma^{(1)} + \kappa^{(2)}\Gamma^{(2)}} \hat{T}_1^\beta, & \text{(A2a)} \\ \hat{T}_\Gamma^{(2)} = \dfrac{\kappa^{(1)}(\Gamma^{(1)} - \beta^{(1)})}{\kappa^{(1)}\Gamma^{(1)} + \kappa^{(2)}\Gamma^{(2)}} \hat{T}_1^\beta. & \text{(A2b)} \end{cases}$$

2. Displacement fields

In the dual space (ω, k_2), the equation of motion, Eq. (2), is a system of two second order differential linear equations with source terms,

$$\begin{pmatrix} \rho^{(i)}\omega^2 - k_2^2 C_{66}^{(i)} + C_{11}^{(i)}\dfrac{\partial^2}{\partial x_1^2} & -jk_2\left(C_{12}^{(i)} + C_{66}^{(i)}\right)\dfrac{\partial}{\partial x_1} \\ -jk_2\left(C_{12}^{(i)} + C_{66}^{(i)}\right)\dfrac{\partial}{\partial x_1} & \rho^{(i)}\omega^2 - k_2^2 C_{22}^{(i)} + C_{66}^{(i)}\dfrac{\partial^2}{\partial x_1^2} \end{pmatrix} \cdot \begin{pmatrix} \hat{u}_1^{(i)} \\ \hat{u}_2^{(i)} \end{pmatrix} = \begin{pmatrix} \lambda_{11}^{(i)}\dfrac{\partial \hat{T}^{(i)}}{\partial x_1} \\ -jk_2\lambda_{22}^{(i)}\hat{T}^{(i)} \end{pmatrix}. \tag{A3}$$

The solution of the system (A3) is the sum of a homogeneous solution $\hat{\mathbf{U}}_h^{(i)}$ and of a particular solution $\hat{\mathbf{U}}_p^{(i)}$. The components of each particular solution $\hat{\mathbf{U}}_q^{(i)}$, $q = \beta^{(i)}, \Gamma^{(i)}$ are obtained by replacing the components of the displacement field $\hat{\mathbf{u}}^{(i)}(x_1)$ by the components of each particular solution $\hat{\mathbf{U}}_q^{(i)}\mathrm{e}^{-qx_1}$ in the system (A3). Each component of the spectrum of the homogeneous solution is expressed as a plane wave

$$\hat{\mathbf{U}}_h^{(i)} = \begin{pmatrix} \hat{U}_1^{(i)} \\ \hat{U}_2^{(i)} \end{pmatrix} \exp\left(-jk_1^{(i)}x_1\right), \tag{A4}$$

where $k_1^{(i)}$ is the projection of the wavevector in direction $\mathbf{x}_1$. This leads to an eigenvalue problem [see Eq. (12) in Ref. 41], where the square roots of the eigenvalues, $k_{n_1}^{(i)}$ and $-k_{n_1}^{(i)}$, stand for wavenumbers of propagating and counter-propagating waves, respectively, and where $n = L, T$ stands for the longitudinal and transverse bulk waves, respectively. The eigenvectors associated to the positive square root of the eigenvalues $k_{n_1}^{(i)}$ are

$$\begin{pmatrix} \hat{U}_{n_1}^{(i)} \\ \hat{U}_{n_2}^{(i)} \end{pmatrix} = \begin{pmatrix} \rho^{(i)}\omega^2 - k_2^2 C_{22}^{(i)} - (k_{n_1}^{(i)})^2 C_{66}^{(i)} \\ k_{n_1}^{(i)} k_2\left(C_{12}^{(i)} + C_{66}^{(i)}\right) \end{pmatrix}. \tag{A5}$$

3. Boundary conditions at the interface

The expressions of the normal $\hat{\sigma}_{11}^{(i)}$ and tangential $\hat{\sigma}_{12}^{(i)}$ stresses are obtained by replacing expressions of the temperature fields $\hat{T}^{(i)}$, Eq. (7), of the particular solutions $\hat{\mathbf{U}}_p^{(i)}$, Eq. (9), and of the homogeneous solutions $\hat{\mathbf{U}}_h^{(i)}$, Eq. (10) into the behavior law, Eq. (3). Thus, the normal stresses $\hat{\sigma}_{11}^{(i)}$ and the tangential stresses $\hat{\sigma}_{12}^{(i)}$ at the interface $x_1 = 0$ are

$$\begin{cases} \hat{\sigma}_{11}^{(i)} = \hat{\sigma}_p^{(i)} + (-1)^i j \sum\limits_{n=L,T} A_n^{(i)}\hat{\zeta}_n^{(i)}, & \text{(A6a)} \\ \hat{\sigma}_{12}^{(i)} = \hat{\tau}_p^{(i)} - \sum\limits_{n=L,T} B_n^{(i)}\hat{\zeta}_n^{(i)}, & \text{(A6b)} \end{cases}$$

where

$$\begin{cases} A_n^{(i)} = C_{11}^{(i)} k_{n_1}^{(i)}\hat{U}_{n_1}^{(i)} + C_{12}^{(i)} k_2 \hat{U}_{n_2}^{(i)}, & \text{(A7a)} \\ B_n^{(i)} = jC_{66}^{(i)}\left(k_2\hat{U}_{n_1} + k_{n_1}^{(i)}\hat{U}_{n_2}^{(i)}\right), & \text{(A7b)} \end{cases}$$

The stresses $\hat{\sigma}_p^{(i)}$ and $\hat{\tau}_p^{(i)}$ associated to the particular solutions are

$$\begin{cases} \hat{\sigma}_p^{(i)} = -\sum\limits_{q=\beta^{(i)},\Gamma^{(i)}} [(-1)^i q C_{11}^{(i)}\hat{U}_{q_1}^{(i)} \\ \quad + jC_{12}^{(i)} k_2 \hat{U}_{q_2}^{(i)} + \lambda_{11}^{(i)}\hat{T}_q^{(i)}], & \text{(A8a)} \\ \hat{\tau}_p^{(i)} = C_{66}^{(i)} \sum\limits_{q=\beta^{(i)},\Gamma^{(i)}} [(-1)^i q \hat{U}_{q_2}^{(i)} - jk_2\hat{U}_{q_1}^{(i)}]. & \text{(A8b)} \end{cases}$$

Taking into account Eqs. (9) and (A6), the boundary conditions, Eq. (11), lead then to the equation

$$\begin{pmatrix} jA_L^{(1)} & jA_T^{(1)} & jA_L^{(2)} & jA_T^{(2)} \\ -jA_L^{(1)} - K_n\hat{U}_{L_1}^{(1)} & -jA_T^{(1)} - K_n\hat{U}_{T_1}^{(1)} & K_n\hat{U}_{L_1}^{(2)} & K_n\hat{U}_{T_1}^{(2)} \\ B_L^{(1)} & B_T^{(1)} & -B_L^{(2)} & -B_T^{(2)} \\ -B_L^{(1)} - K_t\hat{U}_{L_2}^{(1)} & -B_T^{(1)} - K_t\hat{U}_{T_2}^{(1)} & -K_t\hat{U}_{L_2}^{(2)} & -K_t\hat{U}_{T_2}^{(2)} \end{pmatrix} \cdot \begin{pmatrix} \zeta_L^{(1)} \\ \zeta_T^{(1)} \\ \zeta_L^{(2)} \\ \zeta_T^{(2)} \end{pmatrix} = \begin{pmatrix} \hat{\sigma}_p^{(1)} - \hat{\sigma}_p^{(2)} \\ K_n[\hat{U}_{p_1}^{(1)} - \hat{U}_{p_1}^{(2)}] - \hat{\sigma}_p^{(1)} \\ \hat{\tau}_p^{(1)} - \hat{\tau}_p^{(2)} \\ K_t[\hat{U}_{p_2}^{(1)} - \hat{U}_{p_2}^{(2)}] - \hat{\tau}_p^{(1)} \end{pmatrix}. \tag{A9}$$

The solving of Eq. (A9) leads to the expression of $\hat{\zeta}_n^{(i)}$.

[1]W. O. Akande, Y. Cao, N. Yao, and W. Soboyejo, J. Appl. Phys. **107**, 043519 (2010).
[2]J. Uggeri, S. Guizzardi, R. Scandroglio, and R. Gatti, Micron **41**, 210 (2009).
[3]G. Tas, J. J. Loomis, H. J. Maris, A. A. Bailes, and L. E. Seiberling, Appl. Phys. Lett. **72**, 2235 (1998).
[4]J. Wang, R. Weaver, and N. Sottos, Exp. Mech. **42**, 74 (2002).
[5]M. Schoenberg, J. Acoust. Soc. Am. **68**, 1516 (1980).
[6]A. Pilarski and J. L. Rose, J. Appl. Phys. **63**, 300 (1988).
[7]S. I. Rokhlin, J. Acoust. Soc. Am. **89**, 503 (1991).
[8]V. Vlasie and M. Rousseau, Wave Motion **37**, 333 (2003).
[9]V. Vlasie, S. de Barros, M. Rousseau, L. Champaney, H. Duflo, and B. Morvan, Eur. J. Mech. A/Solid **25**, 464 (2006).
[10]M. Castaings, B. Hosten, and D. François, Ultrasonics **42**(4), 1067 (2004).
[11]B. Le Crom and M. Castaings, J. Acoust. Soc. Am. **127**(4), 2220 (2010).
[12]F. Zhang, S. Krishnaswamy, and C. M. Lilley, Ultrasonics **45**, 66 (2006).
[13]S. Delrue and K. Van Den Abeele, Ultrasonics **52**, 315 (2012).
[14]N. Guo and P. Cawley, J. Acoust. Soc. Am. **94**, 2240 (1993).
[15]W. Huang and S. I. Rokhlin, J. Nondestruct. Eval. **11**, 185 (1992).
[16]G. Shkerdin and C. Glorieux, J. Acoust. Soc. Am. **116**, 2089 (2004).
[17]G. S. Murty, J. Acoust. Soc. Am. **58**, 1094 (1975).
[18]T. Hsieh, E. Lindgren, and M. Rosen, Ultrasonics **29**, 38 (1991).
[19]L. J. Pyrak-Nolte, J. Xu, and G. M. Haley, Phys. Rev. Lett. **68**, 3650 (1992).
[20]S. I. Rokhlin and Y. J. Wang, J. Acoust. Soc. Am. **91**, 1875 (1992).
[21]B. W. Drinkwater, R. S. Dwyer-Joyce, and P. Cawley, Proc. R. Soc. London, Ser. A **452**, 2613 (1996).
[22]A. I. Lavrentyev and S. I. Rokhlin, J. Acoust. Soc. Am. **103**, 657 (1998).
[23]M. V. Golub and A. Bostrom, Wave Motion **48**, 105 (2011).
[24]B. Gu, J. Acoust. Soc. Am. **102**, 120 (1997).
[25]G. S. Murty, Phys. Earth Planet. Inter. **11**, 65 (1975).
[26]S. Rokhlin, M. Hefets, and M. Rosen, J. Appl. Phys. **51**, 3579 (1980).
[27]Y. Hu, Y. Liu, and B. Wang, Int. J. Eng. Sci. **48**, 708 (2010).
[28]P. B. Nagy, J. Nondestruct. Eval. **11**, 127 (1992).

[29]L. M. Brock, J. Aust. Math. Soc. Ser. B, Appl. Math. **40**, 72 (1998).
[30]P. C. Vinh and P. T. H. Giang, Wave Motion **48**, 647 (2011).
[31]L. J. Pyrak-Nolte and N. G. W. Cook, Geophys. Res. Lett. **14**, 1107, doi:10.1029/GL014i011p01107 (1987).
[32]J. Du, B. R. Tittmann, and H. S. Ju, Thin Solid Films **518**, 5786 (2010).
[33]T. Dehoux, O. B. Wright, R. L. Voti, and V. E. Gusev, Phys. Rev. B **80**, 235409 (2009).
[34]Q. Han, M. Qian, and H. Wang, Ultrasonics **44**, e1323 (2006).
[35]R. O. Claus and R. A. Kline, J. Appl. Phys. **50**, 8066 (1979).
[36]C. Mattei, X. Jia, and G. Quentin, J. Acoust. Soc. Am. **102**, 1532 (1997).
[37]C. Desmet, V. Gusev, W. Lauriks, C. Glorieux, and J. Thoen, Appl. Phys. Lett. **68**, 2939 (1996).
[38]C. Desmet, V. Gusev, W. Lauriks, C. Glorieux, and J. Thoen, Opt. Lett. **22**, 69 (1997).
[39]C. Glorieux, K. Van de Rostyne, J. Beers, W. Gao, S. Petillion, N. Van Riet, K. Nelson, J. Allard, V. Gusev, W. Lauriks, and J. Thoen, Rev. Sci. Instrum. **74**, 465 (2003).
[40]C. Glorieux, K. V. de Rostyne, J. Goossens, G. Shkerdin, W. Lauriks, and K. A. Nelson, J. Appl. Phys. **99**, 013511 (2006).
[41]J. Higuet, T. Valier-Brasier, T. Dehoux, and B. Audoin, Rev. Sci. Instrum. **82**, 114905 (2011).
[42]B. Audoin and S. Guilbaud, Appl. Phys. Lett. **72**, 774 (1998).
[43]C. Bescond and M. Deschamps, J. Acoust. Soc. Am. **103**, 114 (1998).
[44]J. D. Achenbach, J. Mech. Phys. Solids **51**, 1885 (2003).
[45]B. Audoin, H. Meri, and C. Rossignol, Phys. Rev. B **74**, 214304 (2006).
[46]V. Gusev, J. Acoust. Soc. Am. **100**, 1514 (1996).
[47]C. Glorieux, K. V. de Rostyne, K. Nelson, W. Gao, W. Lauriks, and J. Thoen, J. Acoust. Soc. Am. **110**, 1299 (2001).
[48]J. Zhu, J. S. Popovics, and F. Schubert, J. Acoust. Soc. Am. **116**, 2101 (2004).
[49]B. A. Auld, *Acoustic Fields and Waves in Solids* (R. E. Krierger, Malabar, Florida, 1990), Vol. 1.
[50]M. Perton, "Ultrasons rayonnés par une source laser ponctuelle dans des milieux isotropes transverses et application à la mesure du tenseur d'élasticité de cylindres et de couches minces," Ph.D. dissertation, Université Bordeaux 1, no. 3294 (2006).
[51]G. N. Watson, *A Treatise on the Theory of Bessel Functions* (Cambridge University Press, 1966).
[52]T. Dehoux, N. Chigarev, C. Rossignol, and B. Audoin, Phys. Rev. B **77**, 214307 (2008).
[53]T. Dehoux, M. Perton, N. Chigarev, C. Rossignol, J. M. Rampnoux, and B. Audoin, J. Appl. Phys. **100**, 064318 (2006).
[54]D. H. Hurley, M. Khafizov, and S. L. Shinde, J. Appl. Phys. **109**, 083504 (2011).
[55]D. M. Barnett and J. Lothe, Proc. R. Soc. London, Ser. A **402**, 135 (1985).
[56]D. M. Barnett, Int. J. Solids Struct. **37**, 45 (2000).
[57]T. C. T. Ting, Proc. R. Soc. London, Ser. A **461**, 711 (2005).
[58]M. Destrade and Y. Fu, Int. J. Eng. Sci. **44**, 26 (2006).
[59]D. M. Barnett, S. D. Gavazza, and J. Lothe, Proc. R. Soc. London, Ser. A **415**, 389 (1988).
[60]T. Ting, J. Mech. Mater. Struct. **4**, 631 (2009).
[61]G. D. Meegan, M. F. Hamilton, Y. A. Il'inskii, and E. A. Zabolotskaya, J. Acoust. Soc. Am. **106**, 1712 (1999).
[62]J. Achenbach, *Wave Propagation in Elastic Solids* (North Holland, 1987).
[63]P. Chadwick and P. Borejko, Geophys. J. Int. **118**, 279, (1994).
[64]Y. Chevalier, M. Louzar, and G. Maugin, J. Acoust. Soc. Am. **90**, 3218 (1991).
[65]N. Yoshioka and C. H. Scholz, J. Geophys. Res. **94**, 17681, doi:10.1029/JB094iB12p17681 (1989).
[66]N. Yoshioka and C. H. Scholz, J. Geophys. Res. **94**, 17691, doi:10.1029/JB094iB12p17691 (1989).
[67]S. Biwa, A. Suzuki, and N. Ohno, Ultrasonics **43**, 495 (2005).
[68]C. Rossignol, N. Chigarev, M. Ducousso, B. Audoin, G. Forget, F. Guillemot, and M. C. Durrieu, Appl. Phys. Lett. **93**, 123901 (2008).
[69]L. Hu, X. Zhang, P. Miller, M. Ozkan, C. Ozkan, and J. Wang, J. Appl. Phys. **100**(8), 084701 (2006).